Battery Energy

WILEY

RESEARCH ARTICLE OPEN ACCESS

Amine-Based Chloroaluminate Ionic Liquids as Electrolytes for Aluminium Batteries: A Synthesis and Evaluation Study

C. Zaleski[1,2] | J. Nasterski[1] | A. Garcia-Cruz[2] | J. D. Tinkler[1] | N. Martin-Fabiani[1] | V. Ostanin[3] | E. Piletska[2] | S. Piletsky[2] | S. K. Ghosh[1]

[1]Wolfson School of Mechanical, Electrical and Manufacturing Engineering, Loughborough University, Loughborough, UK | [2]Department of Chemistry, University of Leicester, Leicester, UK | [3]Department of Chemistry, University of Cambridge, Cambridge, UK

Correspondence: S. K. Ghosh (S.Ghosh2@lboro.ac.uk)

Received: 24 October 2024 | **Revised:** 9 September 2025 | **Accepted:** 2 November 2025

Funding: This study was supported by the Strategic Equipment Grant (EP/T006412/1), the DTP Studentship Grant (EP/R513088/1), and EPSRC (Engineering and Physical Sciences Research Council) Research (EP/M027341/1).

ABSTRACT

Amine-based chloroaluminate electrolytes were developed and assessed in this initial feasibility study, the first investigation of this family for aluminium batteries. Primary, secondary, and tertiary amines with different aliphatic chain lengths were evaluated as precursors. Electrochemical performance was measured by potentiometry, real time viscosity changes were probed with a quartz crystal resonator, and aluminium deposit morphology was characterised by optical and atomic force microscopy. Two systems emerged as promising. Triethylamine/$AlCl_3$ remained solid without additives up to 313 K. Under polarisation, quartz crystal resonator measurements showed a sharp, reversible decrease in effective viscosity near the electrode, consistent with a localised potential induced solid to liquid transition reported in ionic liquids, and an associated increase in ionic transport. Dodecylamine, $AlCl_3$ displayed an electrochemical stability window of approximately 1.5 V, comparable to electrolytes already explored for charge storage devices. Both electrolytes exhibited high Faradaic efficiency and redox reversibility, and produced smooth, uniform aluminium deposits. The distinctive features observed here motivate mechanistic studies, long term stability testing, and a systematic survey of amines to develop an optimal solid-state aluminium electrolyte for future devices.

1 | Introduction

Despite significant advancements in lithium-ion battery technology over the last 30 years, sustainability remains a challenge due to issues around electrolyte flammability, ethical mining, raw materials supply chain, and battery recycling. Sustainable electrification demands batteries that deliver high energy density safely and affordably from abundant, recyclable raw materials. Accordingly, research is shifting toward alternative chemistries, particularly recyclable solid-state systems, characterised by low self-discharge and enhanced safety due to reduced electrolyte leakage [1]. The idea of an all-solid-state rechargeable aluminium-ion battery is promising because of the electrochemical, economic, and ecological advantages of aluminium [2]. Electrolytes based on aluminium have a theoretical volumetric capacity four times higher than those based on lithium (Al 8.0 Ah/cm^3 vs. Li 2.0 Ah/cm^3) due to aluminium's three-electron reduction ability while their gravimetric capacities are comparable (Al 3.0 Ah/g vs. Li 3.8 Ah/g) [3]. Aluminium is the most abundant metal in the earth's crust (~8%) with a mature industry and recycling infrastructure that make it economically and ecologically sustainable [4].

1.1 | Suitable Aluminium Electrolyte: A Brief Background

A key hindrance that is yet to be overcome for a prospective aluminium battery is the development of a suitable electrolyte [5–10]. Aqueous aluminium batteries are challenged by aluminium's low cathodic potential (−1.67 V) and high affinity towards oxygen, rendering the electrodeposition of aluminium from aqueous solutions challenging [11]. The research on aluminium battery electrolytes is mostly focused on nonaqueous electrolytes, particularly ionic liquids that have high thermal stability and conductivity [12, 13]. Urea/$AlCl_3$ electrolyte is one of the most studied ionic liquids, alongside other amide-based electrolytes [14, 15]. While amide-based aluminium electrolytes are cost-effective, the presence of an electron-withdrawing carbonyl group reduces the electron density around the nitrogen atom and lowers the affinity of Al-N bond, leading to poor redox kinetics. An alternative approach involves replacing amides with amidine salts resulting in aluminium-to-nitrogen coordination complexes [16, 17]. However, the development of a solid-state aluminium electrolyte that allows for a rapid diffusion of high-valence Al^{3+} ions or an alternative charge transfer mechanism remains a key challenge [18]. Existing efforts have primarily focused on the addition of monomers to already-prepared ionic liquids to create a self-supporting aluminium electrolyte but at the expense of conductivity and diffusion rate [19–22]. In terms of metal–ligand reactions, amines possess several structural advantages over amides and amidines. First, secondary and tertiary amines contain a central nitrogen with multiple hybridisation states, enabling diverse metal–ligand coordination modes. Second, amine basicity generally increases with alkyl substitution, as the electron-donating inductive effect raises electron density at the nitrogen centre, thereby increasing its affinity for metal ions. Neither of these two characteristics are observed with amidines.

1.2 | Aims and Novelty

This study presents the first investigation of amine-based chloroaluminate electrolytes and discusses their potential for application in a solid-state aluminium-ion battery. This paper outlines a simple, safe, and rapid synthesis method involving reactions between aluminium chloride and primary, secondary, and tertiary amines of varying molecular weights (73–185 g mol^{-1}). Previous reports indicated the potential of amines to act as ligands for aluminium, but their use in electrolyte formation required a flammable organic co-solvent, which exacerbated the flammability of the amines [23]. Here, we use amines as ligands for aluminium employing a new, simple and safe synthesis approach to mitigate the amine flammability issue. We prepare the electrolytes without the need for a co-solvent, using a 100% atom economy reaction, which results in a stable, non-flammable electrolyte. Moreover, all amines used in this study, except dodecylamine, are low-density liquids (< 1.2 g cm^{-3}). Consequently, the formation of an ionic electrolyte here is not solely dependent on the lowering of crystal lattice energy of the two starting materials as observed in urea-based chloroaluminate electrolytes. Instead, it largely relies on the dissolution of the metal halide in liquid amine, resulting in significantly faster formation of the electrolyte by approximately 50 times compared to the chloroaluminate electrolyte formation using amides [24].

Primary, secondary, and tertiary amines with a carbon chain length ranging from 4 to 12 were explored in this study. Short-chain amines, particularly methyl- and ethylamine, are gases at ambient temperature, and propylamines are highly volatile, making them impractical for electrolyte preparation. The electrolyte performance was investigated combining potentiometry and quartz crystal resonator, and electrode deposits were characterised using optical microscopy and atomic force microscopy (AFM), as described in "Section 2. Materials and methods." The research led to the discovery of a novel, low-density, self-supporting chloroaluminate electrolyte, triethylamine/$AlCl_3$, that combines attributes of liquid and solid-state systems. The electrolyte remained solid and shape-stable up to 313 K, which may mitigate the leakage and self-discharge associated with liquid electrolytes [25, 26]. Under applied potential, a localised drop in viscosity with enhanced ionic mobility was observed near the electrode, consistent with a potential-induced solid-to-liquid transition reported in ionic liquids [27, 28]. In addition, the dodecylamine/$AlCl_3$ electrolyte exhibited a 1.5 V electrochemical stability window, comparable to electrolytes under investigation for charge storage devices [29]. Both electrolytes showed promising Faradaic efficiency and redox reversibility, and enabled the electrodeposition of smooth, uniform aluminium.

2 | Materials and Methods

2.1 | Electrolyte Preparation

Sigma Aldrich was the source of all the chemicals used in this study, including aluminium chloride, butylamine, diethylamine, triethylamine, tripropylamine, dodecylamine, and decane. All chemicals were used as received. Before preparation of the electrolytes, aluminium chloride was placed under decane to prevent its reaction with atmospheric moisture. Then, the decane/$AlCl_3$ slurry was added slowly to the chosen amine while stirring using a magnetic stirrer (US 152, Stuart), as shown in Figure 1c, resulting in a gradual formation of a liquid electrolyte. This reaction was exothermic, spontaneous and was further intensified by stirring. The reaction flask was cooled to ensure that the temperature did not exceed the boiling point of the amines. This cooling step was not necessary when reacting dodecylamine and $AlCl_3$ because of the high boiling point of dodecylamine (522 K) and its slow reaction rate. All electrolytes were prepared with an excess of $AlCl_3$ at a 1 (amine):1.5 ($AlCl_3$) molar ratio that resulted in compositions containing undissolved metal halide. Thus, this molar ratio was considered to produce a fully saturated electrolyte. Upon completion of the reaction, formed electrolyte separates from decane and remains at the bottom of the reaction flask due to its higher density than decane (circa 1.5 g cm^{-3} vs. 0.78 cm^{-3}). Since decane is not miscible with these electrolytes, purification was deemed unnecessary.

The triethylamine-based electrolyte was gently preheated to 40°C to achieve a fluid state, then introduced into the cylindrical electrolyte compartment of the electrochemical cell (0.23 cm^3). This procedure promoted intimate electrode-electrolyte contact

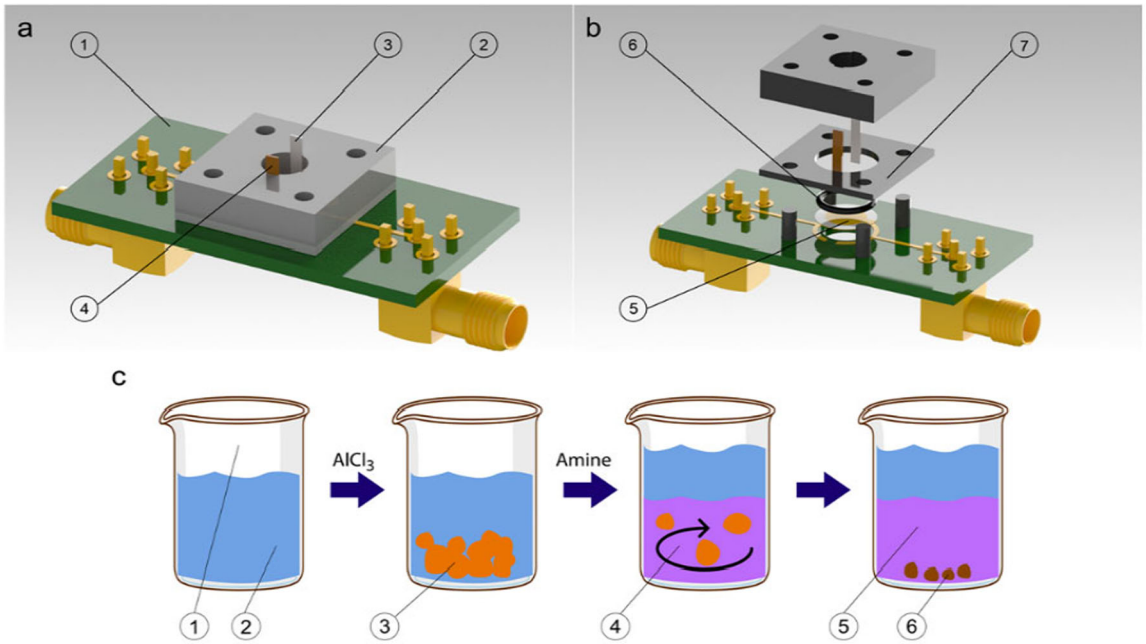

FIGURE 1 | (a). Assembled view of the custom-built electrochemical cell used in the experiments. ①printed circuit board cell housing, ①main body of the cell (3D printed polylactic acid), ③Aluminium foil counter electrode, ④Silver wire reference electrode. (b) Exploded view of the electrochemical cell. ⑤Quartz crystal resonator, QCR (working electrode), ⑥O-ring (Trelleborg AB, Sweden), ⑦O-ring holder plate (polyacrylate). (c) Flow-chart of the electrolyte preparation process. ①reaction vessel, ①decane, ③aluminium chloride/decane slurry, ④formation of chloroaluminate amine electrolyte – enhanced by stirring,⑤formed electrolyte, ⑥unreacted aluminium chloride.

and minimised interfacial resistance before the electrochemical and gravimetric measurements.

2.2 | Electrochemical Quartz Crystal Resonator

Electrochemical experiments were conducted using a custom-built electrochemical cell comprising the cell and a quartz crystal resonator (QCR) as shown in Figure 1a,b. The QCR was used as the cathode during aluminium deposition and the anode during aluminium dissolution. We employed cyclic and linear voltammetry sweeps together with frequency scans of the QCR. Combining electrochemical (potentiometry) and acoustic (QCR) measurements with electrode morphology from optical microscopy and AFM enabled comprehensive characterisation of electrolyte performance and real-time interrogation of interfacial phenomena at the electrode-electrolyte interface.

The electrochemical cell was connected to a Palm Sense 3 potentiostat using custom-built low-pass electronic filters, which removed the interference of the AC potential applied to the QCR on the DC signal recorded by the potentiostat. The working electrode (WE) was the upper gold electrode of an optically polished 14.3 MHz AT-cut QCR, the counter electrode (CE) was an aluminium foil (Goodfellow, UK) and the reference electrode (RE) was a silver wire (Goodfellow, UK). The bottom gold electrode of the QCR was connected to a vector network analyser (VNWA) - DG8SAQ VNWA 3 from SDR-Kits. The VNWA covered a frequency range from 1 kHz to 1.3 GHz, measuring up to 650,000 datapoints with sampling time ranging from 0.13 ms to 100 ms and a dynamic range of 90 dB up to 500 MHz. The QCR admittance (inverse of impedance) data from the VNWA frequency sweep was fitted with the Butterworth–Van Dyke equivalent electrical circuit model of the QCR to determine the changes in resonance frequency and dissipation of the QCR during the electrochemical cycles [30].

2.2.1 | Importance of Viscosity Change and Aluminium Deposit Measurements

The Faradaic efficiency of the electrodeposition process corresponds to the fraction of charge consumed during the reduction reaction at the cathode that is utilised to electrodeposit aluminium. The remaining fraction constitutes electrochemical energy loss. For the viscous electrolytes under consideration, the change in electrolyte viscosity is a key contributor to this energy loss [31]. Hence, to estimate Faradaic efficiency, it is important to measure the mass of aluminium deposit and the viscosity changes in the vicinity of the cathode. In this study, these critical parameters were measured uniquely using the shifts in resonance frequency and acoustic dissipation of the QCR (Section 2.4). Aluminium deposition was quantified at the ends of the reduction and oxidation steps, whereas viscosity was monitored in real-time throughout the process.

The following three different types of electrochemical experiments were used in this study.

Cyclic voltammetry scans were all conducted within the same window (−2 V to 0.5 V) for all the electrolytes to assess the positions of the reduction and oxidation peaks and measure the reduction-to-oxidation window. Each electrolyte was investigated at three different scan rates (5, 2.5 and 1.25 mVs^{-1}) to create Randles-Sevcik plots and use them to calculate the diffusion coefficient of aluminium ions.

Short linear voltammetry sweep experiments were conducted at 1.25 mVs^{-1} from 0.5 to −2 V to record electrochemical and acoustic signatures for each electrolyte during the reduction process only and to obtain a sample of the QCR plated with aluminium. The morphology of the aluminium deposits on the QCR was subsequently studied using optical microscopy and AFM.

A long linear voltammetry sweep experiment was conducted only for triethylamine/$AlCl_3$ electrolyte at a scan rate of 1.25 mVs^{-1} over a narrowed down potential window of 0 V to −0.96 V (for reduction) and return to 0 V (for oxidation) as the bulk of the aluminium depositon and dissolution occurred at this potential range. This experiment served three purposes. The first was to record the real-time electrochemical and acoustic signatures of the electrolyte during reduction and oxidation processes. The second was to collect QCR samples at the ends of reduction (−0.96 V) and oxidation (0 V) to assess the mass and morphology of aluminium deposit using acoustic and AFM readings respectively, and interpret redox reversibility. The voltammetry scan was paused at the end of reduction and oxidation, and the QCR was cleaned and dried to take these measurements. The third purpose was to characterise the potential-induced drop in viscosity and rise in ionic diffusion near the electrodes. Three separate QCRs were employed here for repeats.

Topography images of the QCR surfaces were obtained using a Bruker BioScope Resolve Atomic Force Microscope (AFM) in tapping mode and silicon cantilevers (RTEPSA-525, spring constant 200 N/m, tip radius 8 nm). Images were analysed using NanoScope Analysis 2.0 software.

Optical Microscopy (bright field) images of the aluminium plated QCRs were collected using Nikon SMZ18 optical microscope (at 50× magnification) to estimate the surface coverage for the electrodeposition conducted using each electrolyte (Supporting Information S1: Figure S1).

2.3 | Electrolyte Physical Properties Measurements

The viscosity of the amine/$AlCl_3$ electrolytes before the electrochemical scans was measured using a Bruker Rotational Viscometer of "cup and bob" type (Supporting Information S1: Section S2). The density of the electrolytes was measured using a volumetric cylinder and laboratory balance. The physical properties of the amines and their respective electrolytes used in this study are listed in Supporting Information S1: Table S1. Interestingly, despite having the lowest melting point among the amines studied here, triethylamine formed a solid electrolyte after the addition of $AlCl_3$ and experienced about four-fold increase in viscosity. All other amines, including tripropylamine and dodecylamine with 1.4 times and 1.8 times higher molecular weight than triethylamine respectively, formed liquid electrolytes with $AlCl_3$. We hypothesise that the formation of a solid electrolyte using triethylamine is due to a strong electron donating effect from the three ethyl groups around the central nitrogen atom of this amine, which increases the electron density around the central nitrogen atom and strengthens the Al-N bond. Tripropylamine/$AlCl_3$ electrolyte is liquid at room temperature despite having a stronger electron donating group (propyl), plausibly due to a more dominant steric hindrance effect caused by the presence of a longer alkyl chain.

2.4 | Aluminium Deposit Properties and Real-Time Changes in Electrolyte Viscosity

The mass of aluminium deposit can be estimated in principle from the QCR's resonance frequency shift due to the deposition by applying Sauerbrey Equation [32]. However, the viscous electrolyte couples to the QCR and adds a mass load that varies with viscosity, complicating isolation of the deposit mass from in situ measurements. Hence, the deposit mass was estimated in this study using the difference of the resonance frequency between the two dry states of the QCR, i.e., cleaned of electrolyte, before and after aluminium plating, referred to as 'dry frequency shift' (Δf_{0air}) to distinguish it from the in situ real-time resonance frequency shift measurements. The cleaning was done by submerging the QCR in a 24-well microplate containing 99.5% pure isopropanol and pipetting to create fluid flow. The QCR was then dried in vacuum before reinserting into the electrochemical cell. The mass of aluminium deposit (m_{al}) is given by Equation 1.

$$\frac{\Delta f_{0\text{air}}}{f_{0\text{air}}} = \frac{m_{al}}{A_q t_q \rho_q} \Rightarrow m_{al} = A_q t_q \rho_q \left(\frac{\Delta f_{0\text{air}}}{f_{0\text{air}}} \right) \quad (1)$$

Here, $f_{0\text{air}}$ is the resonance frequency in the dry state before aluminium deposition, A_q is the active area (0.23 cm^2) of the QCR, t_q is the thickness of the QCR (112 μm) and ρ_q is the density of an AT-cut quartz crystal (2.648 g cm^{-3}) [33].

Aluminium deposit thickness was measured using AFM at several locations on the QCR to determine the mean thickness. The deposit surface area was estimated by digitally processing the optical microscopy images using the Image Colour Summariser software (Supporting Information S1: Figure S1), where colour detection was used to estimate the ratio between the areas with clean gold and aluminium deposit. The mean deposit thickness and surface area allowed estimation of aluminium deposit volume. Since the change in electrolyte viscosity is directly proportional to the QCR dissipation, as proven by Kanazawa and Gordon [34], the acoustic dissipation data was used to represent the real-time changes in electrolyte viscosity over the redox cycles (Figure 4).

3 | Results

The results from the multimodal characterisation gave key insights into the electrolyte and aluminium deposit properties.

3.1 | Aluminium Deposit Morphology

Figure 2 and Supporting Information S1: Table S2 depict the morphology of the deposits formed due to the short linear voltammetry sweep experiments going from the oxidative to the reductive state (0.5 to −2 V at 1.25 mVs^{-1}). While all the electrolytes were able to electrodeposit adherent metallic layers, the aluminium deposit from triethylamine/$AlCl_3$ was particularly

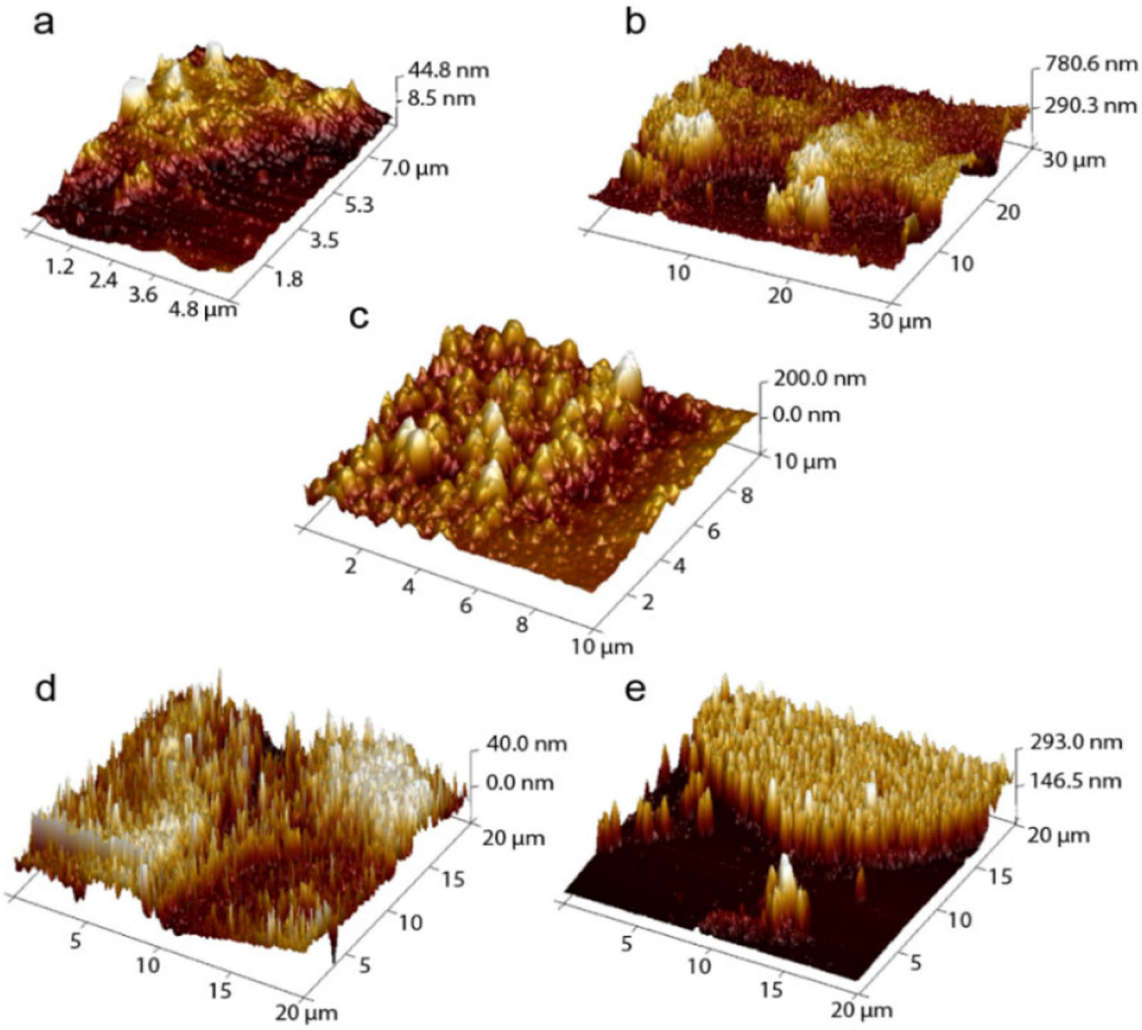

FIGURE 2 | Morphology of the aluminium deposits formed from the following electrolytes, investigated with Atomic Force Microscopy. (a) butylamine/$AlCl_3$, (b) diethylamine/$AlCl_3$, (c) triethylamine/$AlCl_3$, (d) tripropylamine/$AlCl_3$ and (e) dodecylamine/$AlCl_3$. Deposits were obtained during "short linear voltammetry sweeps" conducted from 0.5 to −2 V at 1.25 mV s^{-1} (WE: 14.3 MHz AT-cut Au-plated QCR, CE: Al foil (Goodfellow, UK), RE: Ag wire (Goodfellow, UK)).

noteworthy (Figure 2c). Electroplating using this electrolyte produced a homogeneous layer of aluminium with the highest surface coverage (92%) and second highest thickness (Supporting Information S1: Table S2). The morphology of the deposit also resembled blunt cone-shaped crystals (with lower aspect ratio) rather than sharp needle-like structures observed with the other electrolytes. This is an important finding as needle-like high aspect ratio morphology of electrode deposits has been reported to be prone to dendrite formation [35], a known cause of battery failure. [36–39], The contribution of this potential dendrite-suppression capability on long-term cell stability calls for extensive cycling tests with post-cycling deposit morphology characterisation after identifying suitable electrode materials.

3.2 | Electrochemical Behaviour of Electrolytes

3.2.1 | Redox Reversibility and Faradaic Efficiency

Redox reversibility was noted with triethylamine- and dodecylamine-based electrolytes from the linear and nearly overlapping i_p vs. $v^{1/2}$ plots of the Randles-Sevcik equation (Supporting Information S1: Eq. S1) as shown respectively in Figure 3ii-c, 3ii-e (v: scan rate, i_p: peak current). The ratio of the anodic peak current, $i_{p,\,oxi}$, to the cathodic peak current, $i_{p,\,red}$, was also observed to be close to unity for these two electrolytes, which is consistent with a fully reversible electrochemical process. Moreover, the amounts of charge transferred during the oxidative and reductive processes were observed to be linearly correlated for these two electrolytes (Figure 3iii-c, 3iii-e), which further supported their redox reversibility [40]. Their redox reversibility indicates the potential applicability of these two electrolytes in a rechargeable battery.

While the linear relation between oxidative and reductive charges is strong ($R^2 = 0.994$), this metric alone does not rule out parasitic reactions or structural evolution. It is consistent with high Faradaic efficiency under the present conditions, indicating a prospect for long term stability. Definitive confirmation will require long term cycling studies and complementary measurements, for example electrochemical impedance spectroscopy (EIS) and X-ray photoelectron spectroscopy (XPS).

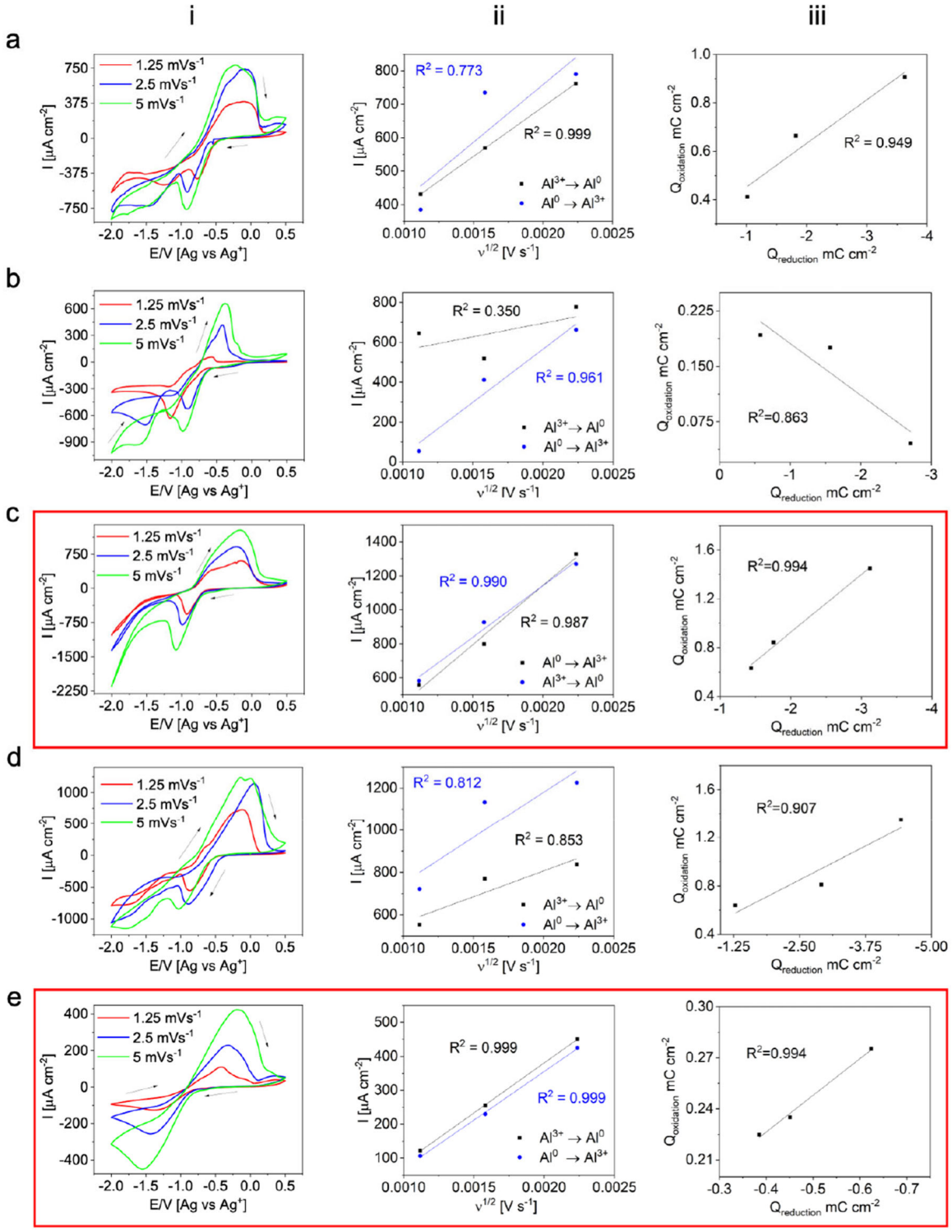

FIGURE 3 | i. Cyclic voltammograms ($\boldsymbol{I}$ vs. $\boldsymbol{E}$) recorded at three scan rates (1.25, 2.5 and 5 mV s^{-1}) for the following electrolytes: (a) butylamine/$AlCl_3$, (b) diethylamine/$AlCl_3$, (c) triethylamine/$AlCl_3$, (d) tripropylamine/$AlCl_3$ and (e) dodecylamine/$AlCl_3$. All experiments were recorded with a WE: 14.3 MHz AT-cut Au-plated quartz crystal, CE : Al foil (Goodfellow, UK), and RE: Ag wire (Goodfellow, UK)). ii. Randles-Sevcik plots ($\boldsymbol{I}$ vs $\boldsymbol{\nu^{1/2}}$) for reduction (black) and oxidation (blue) show reversibility for triethylamine/$AlCl_3$ and dodecylamine/$AlCl_3$. iii. Faradaic efficiency calculated as a ratio between the total amount of charge transferred during oxidation waves ($Q_{oxidation}$) and reduction waves ($Q_{reduction}$) recorded during the cyclic voltammetry sweeps. Symbols represent experimental data points; the line denotes a linear fit to the experimental data. Red outlines show the data for triethylamine and dodecylamine based electrolytes.

3.2.2 | Diffusion-Controlled Kinetics

Since the electrochemical systems investigated in this study display Faradaic charge storage, this suggests that they have diffusion-controlled kinetics. In the cases where linear i_p vs. $v^{1/2}$ plots were obtained from the Randles-Sevcik equation ($R^2 > 0.8$ in Figure 3ii), the correlation coefficient was used to estimate the diffusion coefficient D (Supplementary Information Table S2). The diffusion coefficients derived for diethylamine/$AlCl_3$ (0.88 e-05 mol $m^2 s^{-1}$) and triethylamine/$AlCl_3$ (0.94e-05 mol $m^2 s^{-1}$) electrolytes were nearly two-fold higher than the values reported previously for similar ionic liquids [41]. Remarkably, although the bulk of the triethylamine/$AlCl_3$ electrolyte remained in a solid state during the entire redox cycle, it still provided the fastest diffusion rate. This is consistent with the observations of sharp decrease in acoustic dissipation for triethylamine/$AlCl_3$ (Figure 4c), which suggests localised drop in viscosity near the electrode under potential, facilitating mobility of tightly bound aluminium-amine clusters.

The linearity of the i_p vs. $v^{1/2}$ plots for triethylamine/$AlCl_3$ ($R^2 = 0.987$) and dodecylamine/$AlCl_3$ ($R^2 = 0.999$) (Figure 3ii-c, 3ii-e) also suggest that the mass transfer of aluminium onto the QCR surface is diffusion controlled. Similar observations have been reported for imidazolium-based chloroaluminate electrolytes of comparable viscosities [42] but what sets apart the findings reported here is that triethylamine/$AlCl_3$, despite its high viscosity and shape retaining properties, is capable of maintaining a diffusion rate superior to the imidazolium-based chloroaluminate electrolytes [13].

3.2.3 | Reduction-to-Oxidation Window

Wide electrochemical window (ECW), that is, the maximum potential range outside which the electrolyte undergoes irreversible reduction or oxidation, is a key feature of electrolytes in charge storage devices as the energy stored is proportional to the square of the potential range. Due to experimental limitations, that is, the use of gold-plated QCRs, which are prone to oxidation at higher potentials, only the range between aluminium reduction to oxidation peaks was studied in this work and referred to as the reduction-to-oxidation window. Of the two electrolytes displaying fully reversible redox characteristics, that is, triethylamine/$AlCl_3$ and dodecylamine/$AlCl_3$, the latter displayed a much larger reduction-to-oxidation window of 1.5 V (Figure 3i-e), comparable with those of ionic liquids currently being tested for charge storage devices [43]. Interestingly, the dodecylamine/$AlCl_3$ electrolyte also comprised the longest straight chain amine. This may suggest an influence of the linearity and length of alkyl chains on the reduction-to-oxidation window. However, this correlation needs to be validated through further research involving other long chain amines.

3.2.4 | Potential-Induced Viscosity Decrease—Real-Time QCR Dissipation Studies

The real-time viscosity characteristics of the electrolytes interpreted using shifts in acoustic dissipation, ΔΓ, for three different scan rates (Figure 4-i, ii, iii) were analysed comparatively with their aluminium deposit characteristics (Supporting Information S1: Table S2) and redox reversibility (Figure 3ii). Interestingly, only triethylamine/$AlCl_3$ electrolyte showed a sharp decrease in viscosity immediately after the onset of reduction (at ~900 s in Figure 4c-i, at ~450 s in Figure 4c-ii, and at ~200 s in Figure 4c-iii) with simultaneous increase in current. This viscosity decrease is suggestive of a localised potential-induced solid-to-liquid transition of the electrolyte near the electrode-electrolyte interface as reported in ionic liquids [27, 28]. Freyland and co-workers reported potential-induced phase transitions in [C4mim][PF6] ionic liquids [27]. Ploss et al reported decrease of viscosity of [Emim][Tf2N] ionic liquid on application of potential to the working electrode [28].

We anticipate that the triethylamine/Al^{3+} complex reorients itself on the application of reduction potential with the positively charged Al^{3+} end pointing towards the cathode, thereby facilitating the electrolyte's transition to liquid phase. An alternative hypothesis could suggest that the reduction of Al^{3+} to Al^0 leads to the release of unbound chloride into the electrolyte, potentially resulting in the formation of a solid amine salt (triethylammonium chloride) near the anode, decreasing the electrolyte's viscosity near the cathode. This interesting observation warrants further investigation to confirm the mechanism behind the potential-induced viscosity decrease of triethylamine/$AlCl_3$ near the cathode. It needs to be studied whether the high electron density around the central nitrogen atom due to the three electron donating ethyl groups plays any role in this viscosity decrease.

Decrease in viscosity was also noted for dodecylamine/$AlCl_3$ (Figure 4e) but this occurred at a later phase in the reduction process than triethylamine/$AlCl_3$.

The observation of viscosity decreases for these two electrolytes correlated uniquely with the fact that only these two electrolytes showed full redox reversibility (Figure 3ii-c, 3ii-e) and high volume of aluminium deposit (Supporting Information S1: Table S3). The remaining three electrolytes, butylamine/$AlCl_3$, diethylamine/$AlCl_3$, and tripropylamine/$AlCl_3$, showed viscosity increase after the onset of reduction. Among these three electrolytes, diethylamine/$AlCl_3$ plated the thickest aluminium deposit (Supporting Information S1: Table S2). However, it did not show redox reversibility (Figure 3ii-b), limiting its application in charge storage. The other two electrolytes, butylamine/$AlCl_3$ and tripropylamine/$AlCl_3$, neither plated high volume aluminium deposits (Supporting Information S1: Table S2) nor showed redox reversibility (Figure 3ii-a, 3ii-d). Tripropylamine/$AlCl_3$, which gave the poorest surface coverage of deposit (10%), also displayed the highest increase in viscosity during the reduction process (corresponding to dissipation increase between 60 and 260 kHz depending on the scan rate, Figure 4d).

This analysis demonstrates that the electrolytes that do not undergo an increase in viscosity during the reduction process allow for an efficient electrodeposition and redox reversibility. This observation is intuitive as lower viscosity increases ionic conductivity and mitigates concentration polarisation, reducing ohmic losses and the overpotential required at a given current, thereby improving the energy efficiency of deposition.

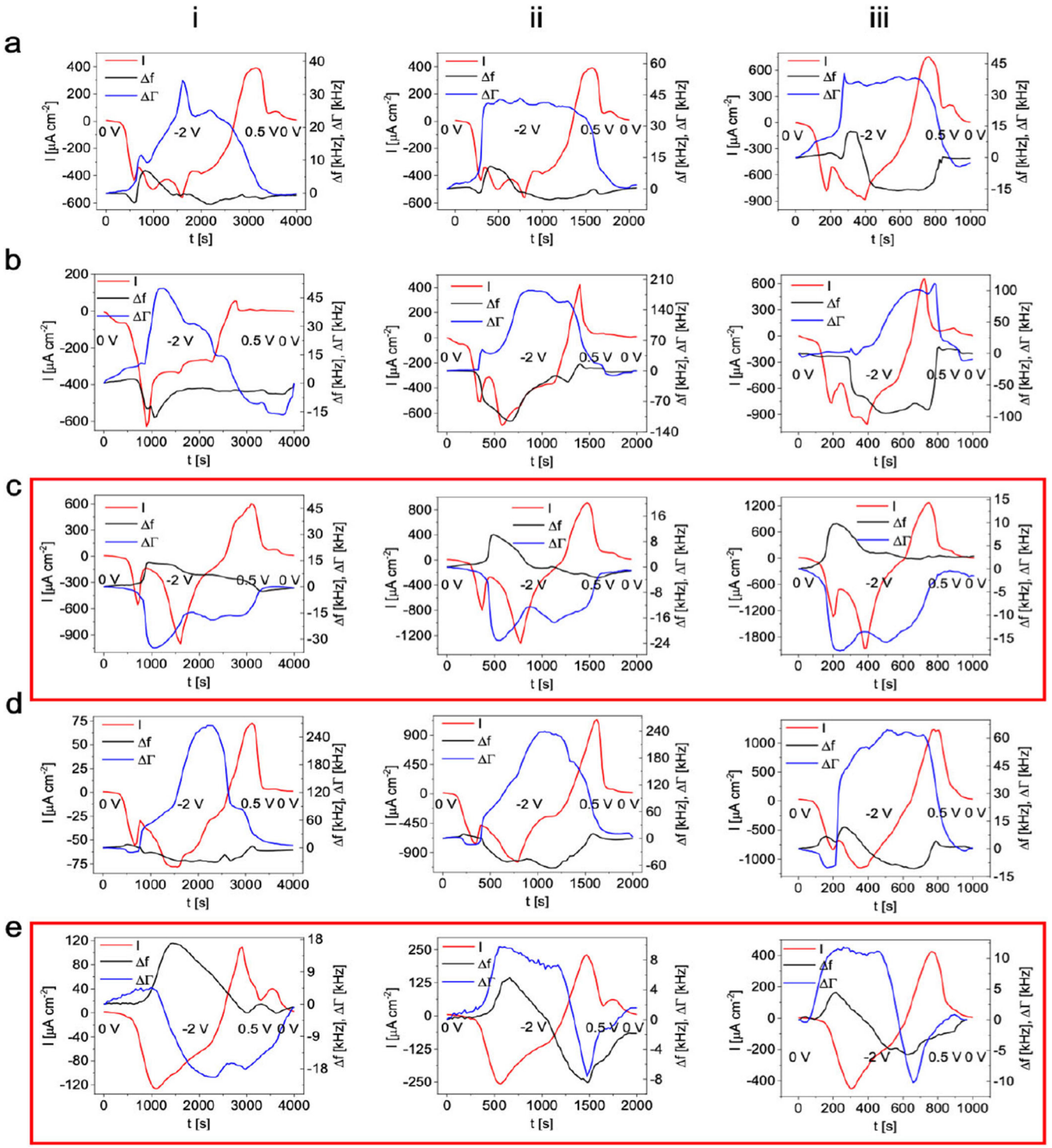

FIGURE 4 | Electrochemical current (I) and shifts in acoustic resonance frequency (Δf) and dissipation (ΔΓ) recorded during cyclic voltammetry expeirments against time. Data shown are from 3rd cyclic voltammogams recored at 1.25 mV s^{-1} (i), 2.5 mV s^{-1} (ii) and 5 mV s^{-1} (iii) for butylamine/$AlCl_3$ (a), diethylamine/$AlCl_3$ (b), triethylamine/$AlCl_3$ (c), tripropylamine/$AlCl_3$ (d) and dodecylamine/$AlCl_3$ (e) (WE: 14.3 MHz AT-cut Au-plated quartz crystal, CE : Al foil (Goodfellow, UK), RE: Ag wire (Goodfellow, UK)). Red outline shows data for triethylamine and dodecylamine based electrolytes.

Increase in scan rate resulted in more pronounced changes in electrolyte viscosity, suggesting the influence of rate of potential change on electrolyte restructuring. Thus, the measurement of QCR dissipation to interpret real-time viscosity changes during the redox cycle shows excellent potential for use as an in-situ real-time indicator of electrolyte performance or electrochemical process diagnostic tool.

3.3 | Results from Short Linear Voltammetry Sweep Experiments

The short linear voltammetry sweep experiments (0.5 to −2 V at 1.25 mVs^{-1}) allowed us to further investigate the aluminium deposit and the electrolyte-electrode phenomena during the reduction phase. The electrolyte viscosity interpreted via QCR

dissipation was observed to increase for all the electrolytes during the reduction phase, with the increase being the earliest for triethylamine/$AlCl_3$ (Supporting Information S1: Figure S3). We attribute this increase in viscosity to the depletion in Al^{3+} ions near the QCR due to their reduction to Al^0. This hypothesis is supported by the observation that the addition of aluminium chloride, i.e., Al^{3+} ions, during electrolyte preparation resulted in viscosity decrease. The viscosity then decreases steeply for triethylamine/$AlCl_3$ consistent with the observations discussed in Section 3.2.

The fact that trietylamine/$AlCl_3$ was the only electrolyte that showed decrease in viscosity (or QCR dissipation) during these short linear voltammetry sweeps (Supporting Information S1: Figure S3) was investigated further during long linear sweep experiments (Section 3.4) as sharp viscosity changes indicates significant changes in Al^{3+} ions concentration in the vicinity of the QCR. This is turn suggested efficient oxidation and reduction for this electrolyte, benefical for charge storage. Faradaic efficiency of electroplating (or plating efficiency) of aluminium from amine-aluminium electrolytes was calculated as the ratio of the charge required to plate the mass of aluminium estimated by the QCR to the overall charge consumed during the reduction reaction estimated from linear voltammetry sweeps. The triethylamine- and dodecylamine-based electrolytes displayed Faradaic efficiency values of 58% and 64.2% respectively (Supporting Information S1: Table S3). Although these values are not as high as those reported for imidazolium-based Al electrolytes [44, 45], they are still encouraging as they were recorded from the electrolytes under ambient condition without using any additives or composition optimisation, which is a scope for our future work [46].

3.4 | Results from Long Linear Voltammetry Sweep Experiments

The redox processes for triethylamine/$AlCl_3$ were investigated further using the long linear voltammetry sweep experiments (0 to −0.96 V and back to 0 V at 1.25 mVs^{-1}). The resonance frequency shift of the QCR at the end of the reduction phase with respect to the unplated state (reference) represent the mass of aluminium deposited. The resonance frequency shift of the QCR at the end of the oxidation phase with respect to the same reference state represent the mass of undissolved aluminium during oxidation. These resonance frequencies were measured in dry states of the QCR, i.e. after cleaning off the electrolyte, as described in Section 2.4 to avoid interference from the viscous electrolyte. Comparison of these resonance frequency shifts indicated that ~75% of the aluminium deposited during reduction dissolved back during oxidation. A comparison of the QCR morphology between the two states obtained using AFM (Supporting Information S1: Figure S4c,d) also showed that a vast majority of the deposited material was removed during the oxidation phase, supporting the QCR data. These QCR and AFM observations confirmed redox reversibility earlier observed in Figure 3ii-c, iii-c. AFM data showed no evidence of dendrite formation in the reduced or oxidised states, suggesting the potential of triethylamine/$AlCl_3$ for secondary charge-storage applications, to be confirmed by extended cycling studies.

The real-time changes in dissipation and resonance frequency shifts of the QCR hold important information on the electrode-electrolyte interface phenomena. The QCR dissipation shift graph (Supporting Information S1: Figure S4a) depicts dramatic changes in viscosity during the redox process. The initial vicosity rise during the reduction phase could be plausibly explained by the depletion of Al^{3+} ions due to aluminium deposition followed by a sharp viscosity decrease at the interface as discussed earlier. The viscosity then rises back steadily during the oxidation phase. The viscosity of the electrolyte/electrode boundary at the end of the experiment (0 V) is marginally higher than that at the start (0 V), plausibly due to lower Al^{3+} concentration arising from residual aluminium on the electrode.

The resonance frequency shift recorded in real-time with the electrolyte in situ at the end state is lower than that at the initial reference state: this can be attributed to the mass of ~25% undissolved aluminium on the QCR and the additional mass coupling from the slightly more viscous electrolyte (due to lower Al^{3+} ions). The resonance frequency shift after reduction compared to the initial state measured with the electrolyte in situ (16 kHz) was greater than the shift between the two states measured with dry QCR (14 kHz), arguably due to the additional mass coupling from the more viscous electrolyte post reduction (due to distinclty lower Al^{3+} ions). Likewise, the difference in the in-situ and dry QCR resonance frequency shifts after oxidation (1 kHz) is attributable to the marginally higher electrolyte viscosity at the end state compared to the initial state (due to slightly lower Al^{3+} ions).

4 | Discussion

Two of the chloroaluminate electrolytes studied here, triethylamine/$AlCl_3$ and dodecylamine/$AlCl_3$, showed some interesting features that may be beneficial for future development of a successful solid-state aluminium battery and merit further investigation. These electrolytes outperformed most ionic liquids reported so far in terms of these features [47]. The electrolytes uniquely showed decrease in viscosity with increase in current during reduction (Figure 4c). The viscosity decrease was primarily near the electrode whereas the bulk of the electrolyte remained in solid-state. This is an important feature as while the interfacial viscosity decrease can allow faster charging, the solid state can limit self-discharge. It may be noted that our inference of viscosity decrease rests on QCR dissipation measurements. Complementing this with real-time morphological changes using in situ optical imaging implanted in a windowed cell may provide definitive evidence of any phase change in the electrolyte state.

The low aspect ratio of aluminium deposits obtained with triethylamine/$AlCl_3$ (Figure 2c) suggests potential for low dendrite formation, contributing to safer battery and faster charging, to be confirmed through further study of long-term charge-discharge cycling once appropriate anode and cathode materials are selected.

The triethylamine/$AlCl_3$ electrolyte exhibited high conductivity despite its solid state with a diffusion rate (~10^{-5} mol m^2 s^{-1} in Supporting Information S1: Table S2) comparable with that of state-of-the-art ionic liquids [45, 48]. Since the redox processes experienced significant viscosity changes, the ionic movement cannot be explained using the Stokes-Einstein equation (Supporting Information S1: Equation S2). Instead, the “Hole

theory" proposed by Abbott and co-workers seems to be a plausible mechanism of ionic movement here [43]. The hole theory stipulates that the ionic mobility is determined by a presence of suitable voids into which ions can move into. The theory postulates the role of ionic liquid density and hole size on ionic mobility (Supporting Information S1: Section S4). The average radius of the holes in an ionic liquid can be calculated using the electrolyte's surface tension. However, further study is required to understand the effects of ionic structure and alkyl chain length on the ionic liquid density and surface tension [49, 50]. The branched structure of triethylamine/$AlCl_3$ with three electron donating methyl groups, causing higher electron density around the central nitrogen atom, could potentially play a role in its high conductivity. Whereas the longer alkyl (propyl) branches of tripropylamine/$AlCl_3$ could potentially contribute to the distribution of species in ionic liquid into polar and nonpolar regions, with the increase in branching of the latter resulting in significant steric hindrance and very low Faradaic efficiency ($< 11\%$, Supporting Information S1: Table S3). On the other hand, the linear nature of the amine chain in dodecylamine/$AlCl_3$ contributed to an encouraging Faradaic efficiency (64%) despite a high chain length, plausibly because the electrochemical energy was used more fruitfully in plating rather than being spent on overcoming steric hindrance within and between the ions.

We observed that linear structure and alkyl chain length of the constituent amines influence the width of the reduction-to-oxidation window of the resulting chloroaluminate electrolytes. For the primary amines studied here, a threefold increase in alkyl chain length from butylamine (C4) to dodecylamine (C12) resulted in twofold ($0.75\,V \rightarrow 1.5\,V$) increase in maximum reduction and oxidation potentials of the corresponding electrolytes. However, the rationale behind this correlation remains unclear and deserves further investigation.

5 | Conclusion and Future Work

The first study on amine-based chloroaluminate electrolytes was presented here with a novel synthesis method and comprehensive characterisation using cyclic and linear voltammetry sweeps, electrochemical quartz crystal resonator, and optical and atomic force microscopy. A range of amines with primary, secondary, and tertiary structures and various chain length was explored as electrolyte precursors. Table 1 summarises the key features of two promising electrolytes, triethylamine/$AlCl_3$ and dodecylamine/$AlCl_3$, discovered in this study and how these features could potentially contribute to a successful solid-state aluminium battery through further exploration of amines based on the current findings, and additive and composition optimisation. These features carry substantial potential and motivate validation through further detailed investigations.

The tertiary amine structure of triethylamine, $AlCl_3$, with electron donating ethyl groups around the central nitrogen, may increase electron density at nitrogen and strengthen Al–N coordination, which could underlie this electrolyte's distinctive features. By contrast, the long chain primary amine dodecylamine, $AlCl_3$ is hypothesised to account for its wide electrochemical stability

TABLE 1 | Summary of features of the most promising amine-aluminium electrolytes from this initial study and their potential contribution to a battery, to be confirmed through further studies.

Electrolyte	Unique features	Potential contribution to a battery
Triethylamine/$AlCl_3$	Remains in solid state until 313 K under no applied potential.	Limit self-discharge in idle state.
	Under applied potential, the viscosity decreases sharply in the vicinity of the electrode with concomitant increase in current.	Higher ionic diffusion/conductivity and faster charging.
	The bulk of electrolyte remains solid, retains shape, when current is drawn from the cell.	Greater safety due to low leakage. Minimise the need for heavy rigid metallic casing, reducing battery weight and contributing to high energy density.
	Shows redox reversibility and promising Faradaic efficiency (58%).	Potential for electrochemical stability, low capacity-fading, high energy density and battery cycle life, to be validated through long-term cycling studies.
	Low aspect ratio of aluminium deposits with no dendrite formation observed.	Potential to avoid catastrophic failure and safety hazards (like fire), not limiting charging speed, to be confirmed via long-term cycling studies.
	High ionic diffusion rate and aluminium deposit coverage area and thickness.	High charge/discharge current, potentially leading to high energy density.
Dodecylamine/$AlCl_3$	Wide reduction-to-oxidation window (1.5 V).	Large electrochemical potential, potentially leading to high energy density.
	Redox reversibility and promising Faradaic efficiency (64%).	Potential for electrochemical stability, low capacity-fading, high energy density and battery cycle life, to be validated through long-term cycling studies.

window. The promising findings of this initial study merit further work, including a systematic survey of branched and straight chain amines to correlate amine structure with electrolyte properties, to elucidate underlying mechanisms, and to evaluate stability through long term cycling. Future work will include extended galvanostatic cycling, impedance tracking, and post cycling analysis of deposit morphology and interfacial chemistry, for example SEM and XPS, to establish cycle life and stability in practical cells.

It is well accepted that no single electrolyte will provide all critical attributes. Establishing structure, property correlations will enable the careful design of a hybrid amine based chloroaluminate electrolyte. The composition of this hybrid electrolyte can be optimised using these amine precursors and additives to achieve the required functional attributes of a solid state aluminium battery, a potentially sustainable alternative to lithium ion batteries in terms of cost, safety, and recyclability [51]. To translate the observed window and redox behaviour into device performance, the next stage will prioritise, mapping the measured stability window to full cell voltage cutoffs and operating temperature to avoid parasitic reactions, pairing the electrolyte with compatible positive electrodes and corrosion resistant current collectors, engineering interfaces by surface treatments, compliant interlayers, modest stack pressure, and controlled preconditioning to minimise contact resistance, tuning electrolyte composition and additives, including amine identity and the $AlCl_3$, amine ratio, to balance stability and transport, and an evaluation plan that progresses from Al, electrolyte, Al symmetric cells to full cells, with extended cycling, rate tests, periodic EIS, coulombic efficiency protocols, and post cycling analysis of interfacial chemistry and deposit morphology, for example SEM and XPS. Evaluating electrolytes in full cell configurations and surveying a range of novel cathode materials remain established approaches for assessing performance under practical operating conditions [52–57]. The successful initial feasibility reported here motivates follow on investigation through these strategies.

Acknowledgements

Authors would like to acknowledge the EPSRC (Engineering and Physical Sciences Research Council) research grant EP/M027341/1 for covering the cost of the acoustic sensor technology development, the Strategic Equipment Grant (EP/T006412/1) for funding the Atomic Force Microscope used in this study, the DTP studentship grant (EP/R513088/1) for James Tinkler, and Loughborough University Doctoral College PhD studentship for Jakub Nasterski.

Conflicts of Interest

The authors declare no conflicts of interest.

Data Availability Statement

The data that support the findings of this study are available from the corresponding author upon reasonable request.

References

1. S. Wang, M. Bai, C. Liu, et al., "Highly Stretchable Multifunctional Polymer Ionic Conductor With High Conductivity Based on Organic-Inorganic Dual Networks," *Chemical Engineering Journal* 440 (2022): 135824.

2. X. Dong, H. Chen, H. Lai, et al., "A Graphitized Expanded Graphite Cathode for Aluminum-Ion Battery With Excellent Rate Capability," *Journal of Energy Chemistry* 66 (2022): 38–44.

3. T. Leisegang, F. Meutzner, M. Zschornak, et al., "The Aluminum-Ion Battery: A Sustainable and Seminal Concept?," *Frontiers in Chemistry* 7 (2019): 268, https://doi.org/10.3389/fchem.2019.00268.

4. C. Exley, "A Biogeochemical Cycle for Aluminium?," *Journal of Inorganic Biochemistry* 97, no. 1 (2003): 1–7.

5. J. Thonstad and S. Rolseth, "Alternative Electrolyte Compositions for Aluminium Electrolysis," *Mineral Processing and Extractive Metallurgy* 114, no. 3 (2005): 188–191.

6. N. Zhu, K. Zhang, F. Wu, Y. Bai, and C. Wu, "Ionic Liquid-Based Electrolytes for Aluminum/Magnesium/Sodium-Ion Batteries," *Energy Material Advances* 2021 (2021): 9204217.

7. K. V. Kravchyk and M. V. Kovalenko, "Aluminum Electrolytes for Al Dual-Ion Batteries," *Communications Chemistry* 3, no. 1 (2020): 120.

8. T. Wei, Z. Wang, Q. Zhang, et al., "Metal–Organic Framework-Based Solid-State Electrolytes for All Solid-State Lithium Metal Batteries: A Review," *CrystEngComm* 24, no. 28 (2022): 5014–5030.

9. Y. Xu, H. Zhang, F. Yang, et al., "State of Charge Estimation of Supercapacitors Based on Multi-Innovation Unscented Kalman Filter under a Wide Temperature Range," *International Journal of Energy Research* 46, no. 12 (2022): 16716–16735.

10. Z. Huang, P. Luo, H. Zheng, and Z. Lyu, "Aluminum-Doping Effects on Three-Dimensional $Li_3V_2(PO_4)_3$@C/CNTs Microspheres for Electrochemical Energy Storage," *Ceramics International* 48, no. 13 (2022): 18765–18772.

11. S. Arshadi Rastabi, G. Razaz, M. Hummelgård, et al., "Metallurgical Investigation of Aluminum Anode Behavior in Water-in-Salt Electrolyte for Aqueous Aluminum Batteries," *Journal of Power Sources* 523 (2022): 231066.

12. K. K. Maniam and S. Paul, "A Review on the Electrodeposition of Aluminum and Aluminum Alloys in Ionic Liquids," *Coatings* 11, no. 1 (2021): 80.

13. R. Böttcher, A. Ispas, and A. Bund, "Determination of Transport Parameters In [EMIm]Cl–Based Ionic Liquids – Diffusion and Electrical Conductivity," *Electrochimica Acta* 366 (2021): 137370.

14. Y. Bian, Y. Li, Z. Yu, et al., "Using an AlCl3/Urea Ionic Liquid Analog Electrolyte for Improving the Lifetime of Aluminum-Sulfur Batteries," *ChemElectroChem* 5, no. 23 (2018): 3607–3611.

15. M. Angell, C. J. Pan, Y. Rong, et al., "High Coulombic Efficiency Aluminum-Ion Battery Using an AlCl3-Urea Ionic Liquid Analog Electrolyte," *Proceedings of the National Academy of Sciences of the United States of America* 114, no. 5 (2017): 834–839.

16. A. J. Lucio, I. Efimov, O. N. Efimov, et al., "Amidine-Based Ionic Liquid Analogues With AlCl3: A Credible New Electrolyte for Rechargeable Al Batteries," *Chemical Communications* 57, no. 77 (2021): 9834–9837.

17. O. O. Okoturo and T. J. VanderNoot, "Temperature Dependence of Viscosity for Room Temperature Ionic Liquids," *Journal of Electroanalytical Chemistry* 568 (2004): 167–181.

18. D.-Y. Wang, C. Y. Wei, M. C. Lin, et al., "Advanced Rechargeable Aluminium Ion Battery With a High-Quality Natural Graphite Cathode," *Nature Communications* 8, no. 1 (2017): 14283.

19. X.-G. Sun, Y. Fang, X. Jiang, K. Yoshii, T. Tsuda, and S. Dai, "Polymer Gel Electrolytes for Application in Aluminum Deposition and Rechargeable Aluminum Ion Batteries," *Chemical Communications* 52, no. 2 (2016): 292–295.

20. Á. Miguel, N. García, V. Gregorio, A. López-Cudero, and P. Tiemblo, "Tough Polymer Gel Electrolytes for Aluminum Secondary Batteries Based on Urea: $AlCl_3$, Prepared by a New Solvent-Free and Scalable Procedure," *Polymers* 12, no. 6 (2020): 1336.

21. T. Schoetz, O. Leung, C. P. de Leon, C. Zaleski, and I. Efimov, "Aluminium Deposition in EMImCl-$AlCl_3$ Ionic Liquid and Ionogel for Improved Aluminium Batteries," *Journal of The Electrochemical Society* 167, no. 4 (2020): 040516.

22. A. Lewandowski, "New Composite Solid Electrolytes Based on a Polymer and Ionic Liquids," *Solid State Ionics* 169, no. 1 (2004): 21–24.

23. I. A. Menzies and D. B. Salt, "The Electrodeposition of Aluminium," *Transactions of the IMF* 43, no. 1 (1965): 186–191.

24. N. Canever, N. Bertrand, and T. Nann, "Acetamide: A Low-Cost Alternative to Alkyl Imidazolium Chlorides for Aluminium-Ion Batteries," *Chemical Communications* 54, no. 83 (2018): 11725–11728.

25. Z. Li, S. Weng, J. Fu, et al., "Nonflammable Quasi-Solid Electrolyte for Energy-Dense and Long-Cycling Lithium Metal Batteries With High-Voltage Ni-Rich Layered Cathodes," *Energy Storage Materials* 47 (2022): 542–550.

26. Z. Huang, W. L. Song, Y. Liu, et al., "Stable Quasi-Solid-State Aluminum Batteries," *Advanced Materials* 34, no. 8 (2022): 2104557.

27. W. Freyland, "Interfacial Phase Transitions in Conducting Fluids," *Physical Chemistry Chemical Physics* 10, no. 7 (2008): 923–936.

28. M. A. Ploss, M. W. Rutland, and S. Glavatskih, "Influence of Electric Potential on the Apparent Viscosity of an Ionic Liquid: Facts and Artifacts," *Physical Chemistry Chemical Physics* 18, no. 38 (2016): 26609–26615.

29. A. J. Lucio, I. Sumarlan, E. Bulmer, et al., "Measuring and Enhancing the Ionic Conductivity of Chloroaluminate Electrolytes for Al-Ion Batteries," *Journal of Physical Chemistry C* 127, no. 28 (2023): 13866–13876.

30. A. Guha, N. Sandström, V. P. Ostanin, W. van der Wijngaart, D. Klenerman, and S. K. Ghosh, "Simple and Ultrafast Resonance Frequency and Dissipation Shift Measurements Using a Fixed Frequency Drive," *Sensors and Actuators B: Chemical* 281 (2019): 960–970.

31. A. Kumar and D. Sarma, "Recent Applications of Chloroaluminate Ionic Liquids in Promoting Organic Reactions." *Ionic Liquids IIIB: Fundamentals, Progress, Challenges, and Opportunities* (American Chemical Society, 2005), 350–370.

32. G. Sauerbrey, "Verwendung Von Schwingquarzen Zur Wägung Dünner Schichten Und Zur Mikrowägung," *Zeitschrift für Physik* 155, no. 2 (1959): 206–222.

33. M. Rodahl, F. Höök, and B. Kasemo, "QCM Operation in Liquids: An Explanation of Measured Variations in Frequency and Q Factor With Liquid Conductivity," *Analytical Chemistry* 68, no. 13 (1996): 2219–2227.

34. K. Keiji Kanazawa and J. G. Gordon, "The Oscillation Frequency of a Quartz Resonator in Contact With Liquid," *Analytica Chimica Acta* 175 (1985): 99–105.

35. Y. Long, H. Li, M. Ye, et al., "Suppressing Al Dendrite Growth Towards a Long-Life Al-Metal Battery," *Energy Storage Materials* 34 (2021): 194–202.

36. X. Ke, Y. Wang, L. Dai, and C. Yuan, "Cell Failures of All-Solid-State Lithium Metal Batteries With Inorganic Solid Electrolytes: Lithium Dendrites," *Energy Storage Materials* 33 (2020): 309–328.

37. J. W. Gibbs, K. A. Mohan, E. B. Gulsoy, et al., "The Three-Dimensional Morphology of Growing Dendrites," *Scientific Reports* 5, no. 1 (2015): 11824.

38. J. Zheng, D. C. Bock, T. Tang, et al., "Regulating Electrodeposition Morphology in High-Capacity Aluminium and Zinc Battery Anodes Using Interfacial Metal–Substrate Bonding," *Nature Energy* 6, no. 4 (2021): 398–406.

39. A. Hagopian, M.-L. Doublet, and J.-S. Filhol, "Thermodynamic Origin of Dendrite Growth in Metal Anode Batteries," *Energy & Environmental Science* 13, no. 12 (2020): 5186–5197.

40. R. Zhang, G. van Straaten, V. di Palma, et al., "Electrochemical Activation of Atomic Layer-Deposited Cobalt Phosphate Electrocatalysts for Water Oxidation," *ACS Catalysis* 11, no. 5 (2021): 2774–2785.

41. K. Hayamizu, Y. Aihara, H. Nakagawa, T. Nukuda, and W. S. Price, "Ionic Conduction and Ion Diffusion in Binary Room-Temperature Ionic Liquids Composed of [emim][BF4] and LiBF4," *Journal of Physical Chemistry B* 108, no. 50 (2004): 19527–19532.

42. Q. Wang, Q. Zhang, X. Lu, and S. Zhang, "Electrodeposition of Al From Chloroaluminate Ionic Liquids With Different Cations," *Ionics* 23, no. 9 (2017): 2449–2455.

43. D. R. MacFarlane, et al., "Energy Applications of Ionic Liquids," *Energy & Environmental Science* 7, no. 1 (2014): 232–250.

44. K. L. Ng, B. Amrithraj, and G. Azimi, "Nonaqueous Rechargeable Aluminum Batteries," *Joule* 6, no. 1 (2022): 134–170.

45. Y. Peng, P. S. Shinde, and R. G. Reddy, "Diffusion Coefficient and Nucleation Density Studies on Electrochemical Deposition of Aluminum From Chloroaluminate Ionic Liquid Electrolytes," *Journal of Electroanalytical Chemistry* 895 (2021): 115363.

46. A. Abbott, J. C. Barron, M. Elhadi, et al., "Electrolytic Metal Coatings and Metal Finishing Using Ionic Liquids," *ECS Transactions* 16, no. 36 (2009): 47–63.

47. M. Galiński, A. Lewandowski, and I. Stępniak, "Ionic Liquids as Electrolytes," *Electrochimica Acta* 51, no. 26 (2006): 5567–5580.

48. V. A. Elterman, P. Y. Shevelin, L. A. Yolshina, and A. V. Borozdin, "Features of Aluminum Electrodeposition From 1,3-dialkylimidazolium Chloride Chloroaluminate Ionic Liquids," *Journal of Molecular Liquids* 351 (2022): 118693.

49. M. González-Melchor, F. Bresme, and J. Alejandre, "Molecular Dynamics Simulations of the Surface Tension of Ionic Liquids," *Journal of Chemical Physics* 122, no. 10 (2005): 104710.

50. C. Kolbeck, J. Lehmann, K. R. J. Lovelock, et al., "Density and Surface Tension of Ionic Liquids," *Journal of Physical Chemistry B* 114, no. 51 (2010): 17025–17036.

51. J. Janek and W. G. Zeier, "A Solid Future for Battery Development," *Nature Energy* 1, no. 9 (2016): 16141.

52. Z. Meng, Z. Qiu, Y. Shi, et al., "Micro/Nano Metal–Organic Frameworks Meet Energy Chemistry: A Review of Materials Synthesis and Applications," *eScience* 3, no. 2 (2023): 100092.

53. Z. Hui, J. An, J. Zhou, W. Huang, and G. Sun, "Mechanisms for Self-Templating Design of Micro/Nanostructures Toward Efficient Energy Storage," *Exploration* 2, no. 5 (2022): 20210237.

54. H. Song, Y. Wang, Q. Fei, D. H. Nguyen, C. Zhang, and T. Liu, "Cryopolymerization-Enabled Self-Wrinkled Polyaniline-Based Hydrogels for Highly Stretchable All-in-One Supercapacitors," *Exploration* 2, no. 4 (2022): 20220006.

55. S. Wang, S. Xiao, S. Li, et al., "Organic Cationic-Coordinated Perfluoropolymer Electrolytes With Strong Li^+-Solvent Interaction for Solid State Li-Metal Batteries," *Angewandte Chemie International Edition* 63, no. 52 (2024): e202412434, https://doi.org/10.1002/anie.202412434.

56. L. Zhang, S. Wang, Q. Wang, H. Shao, and Z. Jin, "Dendritic Solid Polymer Electrolytes: A New Paradigm for High-Performance Lithium-Based Batteries," *Advanced Materials* 35, no. 35 (2023): 2303355.

57. C. Liu, S. Wang, X. Wu, et al., "In Situ Construction of Zwitterionic Polymer Electrolytes With Synergistic Cation–Anion Regulation Functions for Lithium Metal Batteries," *Advanced Functional Materials* 34, no. 1 (2024): 2307248.

Supporting Information

Additional supporting information can be found online in the Supporting Information section.
SI AmineAlElectrolyte Submitted.